



HAL
open science

Analyse fréquentielle des débits de crues avec des données historiques en prenant en compte les erreurs aléatoires et systématiques

Luc Neppel, Benjamin Renard, Michel Lang, Pierre Alain Ayrat, Denis Coeur, Eric Gaume, Nicolas Jacob, Olivier Payrastre, Karine Pobanz, Freddy Vinet

► To cite this version:

Luc Neppel, Benjamin Renard, Michel Lang, Pierre Alain Ayrat, Denis Coeur, et al.. Analyse fréquentielle des débits de crues avec des données historiques en prenant en compte les erreurs aléatoires et systématiques. *Hydrological Sciences Journal*, 2010, 55 (2), pp 192-208. 10.1080/02626660903546092 . hal-00509088

HAL Id: hal-00509088

<https://hal.science/hal-00509088>

Submitted on 15 May 2020

HAL is a multi-disciplinary open access archive for the deposit and dissemination of scientific research documents, whether they are published or not. The documents may come from teaching and research institutions in France or abroad, or from public or private research centers.

L'archive ouverte pluridisciplinaire **HAL**, est destinée au dépôt et à la diffusion de documents scientifiques de niveau recherche, publiés ou non, émanant des établissements d'enseignement et de recherche français ou étrangers, des laboratoires publics ou privés.

1 **Flood frequency analysis using historical data: accounting for random and systematic**
2 **errors**

3

4 LUC NEPPEL¹, BENJAMIN RENARD², MICHEL LANG², PIERRE-ALAIN AYRAL³,
5 DENIS COEUR⁴, ERIC GAUME⁵, NICOLAS JACOB⁶, OLIVIER PAYRASTRE⁷, KARINE
6 POBANZ², FREDDY VINET⁸.

7 1 UMR HydroSciences Montpellier – Université Montpellier II – place Eugène Bataillon – CC MSE – 34090
8 Montpellier Cedex 5, France. – neppel@msem.univ-montp2.fr

9 2 Cemagref Lyon – Hydrology Hydraulics – 3 bis quai Chauveau – CP 220 – 69336 Lyon cedex 09, France.

10 3 Ecole des Mines d'Alès, LGEI, 6 av de Clavières, 30 100 Alès, France

11 4 ACTHYS Diffusion, 253, chemin de Plate-Rousset, 38 330 Biviers, France

12 5 LCPC, Route de Bouaye, BP 4129, 44341 Bouguenais cedex, France

13 6 Université de Lyon II - UMR 5600 – 5 avenue Pierre Mendès –France 69676 Bron cedex, France

14 7 SPC Grand Delta du Rhone, DDE du Gard, 89, rue Weber, 30907 Nimes cedex, France

15 8 UMR Gester,, Université Montpellier III, Route de Mende, 34199 Montpellier Cedex 5, France

16 **Abstract :**

17

18 This paper presents a flood frequency analysis (FFA) based on a set of systematic data and a
19 set of historical floods, applied to several Mediterranean catchments. After identification and
20 collection of data on historical floods, several hydraulic models were constructed to account
21 for geomorphological changes. Recent and historical rating curves were constructed and
22 applied to reconstruct flood discharge series along with their uncertainty. This uncertainty
23 stems from two types of errors: (a) random errors related to the water level readings; (b)
24 systematic errors related to over- or underestimation of the rating curve. A Bayesian
25 frequency analysis is performed to take both sources of uncertainty into account. It is shown
26 that: (a) the uncertainty affecting discharges should be carefully evaluated and taken into
27 account in the FFA, as it can increase the quantiles confidence interval; (b) the quantiles are

28 found consistent with the ones obtained with empirical methods, for two out of four of the
29 catchments.

30

31 **Keyword :**

32

33 Historical flood, Bayesian flood frequency analysis, discharge errors, Mediterranean
34 catchment

35

36 **I. INTRODUCTION**

37

38 The most widely used method for flood frequency analysis is to estimate the parameters of a
39 probability distribution using a sample of observed flood events. As discharge time series are
40 often short compared to the recurrence interval of the quantiles of interest, this method is
41 highly sensitive to the sampled data. In France, for example, the longer uninterrupted
42 discharge series provide 40 to 50 years of data, with only a couple of series longer than 80
43 years (Renard, 2006), whereas flood-risk areas are defined on the basis of a design event with
44 a recurrence interval of at least 100 years. One way of reducing the resulting uncertainties is
45 to extend the observation period by augmenting the systematic observations with historical
46 flood events or paleofloods. A number of applications – for example, Llasat *et al.* (2005) in
47 Catalonia; Naulet *et al.* (2005) on the Ardèche river (France); and Payrastre *et al.* (2005,
48 2006) on small watersheds in the Aude river system (France) – demonstrate the improvement
49 offered by this method compared to methods using only the systematic observation period.
50 Brazdil *et al.* (2006) provide a more detailed assessment of flood risk that takes account of
51 historical flood events in Europe.

52 A first difficulty with this approach lies in the estimation of empirical flood frequencies from
53 a sample made of both systematic and censored data. Indeed, historical discharge data are not
54 exhaustive: only events exceeding a given threshold of perception (possibly varying over
55 time) are reported. Hirsh and Stedinger (1987) and Naulet (2002) propose ways of computing
56 empirical flood frequencies with a mixed systematic/censored sample. A second difficulty is
57 to quantify the discharge of historical flood events, as this information is often subject to
58 considerable uncertainty, which must be taken into consideration in estimating flood
59 frequency. Moreover, such error is not limited to historical floods; it also affects more recent
60 exceptional events for which only posterior estimates of discharge are available (Gaume *et al.*,
61 2004; Sheffer *et al.*, 2008). It can be considered that the data on historical flood events are
62 marred by random errors related to readings of the staff gauge, and both historical and recent
63 flood events are marred by systematic errors arising from over- or underestimation of the
64 rating curve.

65 This paper presents a frequency analysis method that takes these two sources of error into
66 account for floods in both the historical and systematic periods. The approach presented was
67 developed under the INONDHIS-LR project (Neppel *et al.*, 2007), funded by the French
68 Ministry of Ecology. The second section presents the study area and the data. The third
69 section describes the frequency analysis models, with an application to a Mediterranean
70 catchment. The results of the analysis are further discussed in the fourth section.

71

72 **II. STUDY AREA AND DATA**

73

74 **1. Location of the study area**

75

76 The INONDHIS-LR project studies ten Mediterranean catchments: two in the Hérault river
77 system, four in the Aude and four in the Gard watershed. This paper considers the latter
78 catchments, particularly the catchment of the Gardon d'Anduze river at Anduze, which has an
79 area of 540 km², making it – along with the Gardon d'Alès (320 km²) – one of the main
80 tributaries of the Gard river, which drains a total area of about 2000 km² into the Rhône river
81 (Figure 1).

82

83 The two main tributaries of the Gardon d'Anduze are the Gardon de Saint-Jean (154 km²) and
84 the Gardon de Mialet (219 km²). Their catchments are bounded on the north by the crests of
85 the Cévennes range, which can exceed 1000 mNGF¹ in altitude, and their outlets lie at
86 altitudes around 100 m. Given the steep gradients of the catchments and the torrential rainfall
87 characteristic of the Mediterranean rim in autumn, these streams are the site of devastating
88 floods (Ayrat, 2004; Marchandise, 2007).

89

90 The four catchments in the Gard system are instrumented by gauging stations belonging to the
91 Grand Delta flood forecasting department (FFD), formerly the flood warning department
92 (FWD), founded in 1892. The purpose of these measurements was not to compile a time
93 series of discharge data for hydrological analysis, but to provide flood warning. Managers
94 were therefore interested in the flood crest levels rather than in discharge *per se*, which
95 explains the virtual absence of gaugings (there are only two low-flow gaugings at the Anduze
96 station). The possibilities for gauging discharge during flood events are severely limited by
97 the high flow velocity. Incidentally, this is why a majority of hydrometric stations in the
98 Mediterranean region are not gauged beyond the 2-year flood (Lang *et al.*, 2006). The Grand
99 Delta FFD allowed the authors of this paper to use the topographical surveys conducted in

¹ NGF = *nivellement général de la France*, the altitude reference system of France's National Geographical Institute (IGN).

100 2003 for all catchments in the Gard river system, with longitudinal profiles and latitudinal
101 profiles from 40 to 300 metres apart.

102

103 **2. Available historical data**

104

105 The work of identifying historical information, collecting it from archives and subjecting it to
106 critical analysis was conducted in conjunction with historians and geographers. The methods
107 used are not described in this paper; for a description, see Cœur *et al.* (2002) or Naulet *et al.*
108 (2005). The data relate either to flood crest levels or to the morphology of the Gardon.

109

110 For this sector, a total of 249 useable flood crest measurements were found, the oldest dating
111 from 1741. When their positions were given with respect to a landmark still in existence, it
112 became possible to place them in the NGF system. Some archives provided only censored
113 information owing to the lack of precision of observations, e.g. “the water level is above the
114 bridge parapet”. Figure 2 lists all the flood events found for the Gardon d’Anduze; the series
115 is incomplete for the 1741-1891 period (high water mark, threshold level not exceeded,
116 measurement recorded as an interval) and complete since 1892. The FFD archives contributed
117 greatly: the entire series of daily water-level measurements were found for the four
118 catchments studied, dating back to the founding of FWD in 1892. The past positions and zero
119 levels of the staff gauges were reconstructed, partly from correspondence between FFD
120 engineers and the observers assigned to each sector, and partly from breaks in the time series
121 of low-water levels.

122

123 Historical information on the morphology of the Gardon stems from technical studies for
124 hydraulic works and reports on major hydrometeorological events. The plans, consisting of

125 longitudinal profiles and a few latitudinal profiles, show the crest levels of known major flood
126 events. The period from 1845-1850 to the present, was marked by a deepening of the
127 streambeds, by more than three metres in some areas. This phenomenon, which has also been
128 evidenced in a nearby area through analysis of lichens (Gob *et al.*, 2008), results from an
129 incision in the gravelly alluvium and the gradual scouring out of this material once
130 sedimentary build-up in the channels stopped in these catchments. As in most watercourses in
131 the Rhône watershed, the process seems irreversible as from the 1950s. Figure 3 presents a 3
132 km stretch of the Gardon d'Anduze at Anduze. Comparing the oldest useable profile, dating
133 from 1849, to that produced in the 2003 survey, it can be seen that the river bed has sunk by
134 approximately 2 m on the downstream side of the Anduze bridge.

135

136 **3. Example of reconstruction of flood discharges at Anduze**

137

138 Estimates of flood discharge are based on hydraulic modelling of a reach about 2 km long.
139 The river bed was fairly stable at the downstream end between the 1849 and 1985 profiles
140 (Figure 3), then deepened by about 1.5 m between 1985 and 2003. We therefore use two
141 models: a “recent” model based on the 2003 topographical surveys supplemented by
142 Cemagref's 2006 surveys and applied to the period from 1985 onward; and a “historical”
143 model obtained by raising the river bed floor by 1.50 m. Considering the consistency between
144 1849 and 1985 profiles, the latter is considered to be representative of the streambed
145 topography for the historical period. The historical profiles collected did not allow to
146 reconstruct the river's topographical past with sufficient precision to refine the hydraulic
147 models further.

148

149 Discharge estimates are based on numerical solutions of Barré de Saint Venant's free surface
150 runoff equations (Chow, 1960), in a one-dimensional simulation using the Manning-Strickler
151 discharge formula. The software used was RUBARBE (Paquier and Khodashenas, 2002),
152 which divides the river's geometry into a low flow channel and a floodplain. The software
153 makes it possible to model a change from sub-critical flow to torrential flow.

154

155 The first step in hydraulic modelling is to calibrate the model, i.e. to determine the Manning
156 coefficients. The calibration procedure is performed in two steps (main channel/floodplain),
157 and is described in greater detail in Renouf *et al.* (2005) and Lang *et al.* (2006). For the main
158 channel, calibration is performed using stream gaugings. A first Manning coefficient is
159 estimated based on the (water level;discharge) observations. An uncertainty of +/-5 cm for
160 water level and +/-10% for discharge is then considered. A second calibration procedure is
161 performed using the values (water level minus 5 cm, discharge plus 10%) and (water level
162 plus 5 cm, discharge minus 10%). This leads to an interval for the Manning coefficient in the
163 main channel, which corresponds to an envelop curve of the rating curve (Figure 4). This
164 approach is applied with two gaugings available at Anduze, corresponding to low discharges
165 in the main channel. The corresponding Manning coefficient ranges from 1/30 to 1/20. In the
166 floodplain, no measurements were available, so the Manning coefficient is restricted to the
167 interval 1/20- 1/10, based on field observations and the configuration of the floodplain (see
168 correspondence tables, Barnes, 1967).

169

170 The second step is to construct rating curves in the staff gauge cross-section. For each model
171 (historical and recent), the primary relationship between discharge and water level is
172 determined, then a range for this relationship is derived from the uncertainty bounds on the
173 Manning coefficient, as explained on figure 4. Figure 5 presents the rating curves obtained.

174 One can notice on figure 5 that the upper limit of the rating curve described by the rating
175 curve error model doesn't correspond to the previous one by hydraulic sensitivity analysis (i.e
176 the envelop curve related to the sensitive analysis on Manning coefficient). The hydraulic
177 analysis showed that if supercritical flow appears in the neighbourhood of the bridge for the
178 three curves (respect. upper, central and lower) for respectively $Q = 4000$, 5000 and 6000
179 m^3/s , the position of the hydraulic jump is either just in front of the flood scale (upper curve)
180 or upstream the flood scale (central and lower curves). The former case leads to an equivocal
181 relationship between stage and discharge, but a large uncertainty remains on the exact
182 location of the hydraulic jump. As such hypothetical upper limit yields values that are much too
183 high in terms of specific discharge, it has been considered to be overestimated. The rating
184 curve error model was therefore calibrated without hydraulic jump.

185
186 Once the rating curves have been constructed for both the recent and historical models, the
187 sample of flood level measurements is used to construct the sample of discharge values.
188 Figure 2 shows the series of reconstructed discharge values from 1741 to 2005. Discharges
189 have been estimated using the central rating curves in figure 5 (the uncertainty related to a
190 possible systematic rating curve error is therefore not represented in figure 2). It can be
191 observed that this data series is made of several data types:

- 192 • Point-values (circles) correspond to water level data known with high precision.
193 Discharges corresponding to such data are therefore solely affected by the uncertainty
194 stemming from rating curve errors (not represented in figure 2).
- 195 • Intervals correspond to water level data known with limited precision. The
196 information therefore consists of lower and upper bounds for the water level reached
197 during the flood. This water level interval can be transformed into a discharge interval
198 using the central rating curve.

- 199 • The perception threshold (horizontal line) corresponds to the water level ensuring the
200 exhaustiveness of historical data collection. In other words, it can be ensured that
201 water levels did not exceed the perception threshold during years with no available
202 information in figure 2 (otherwise, such event would have been recorded in the
203 historical archives).

204

205 The five highest flood levels recorded at Anduze are those of 1958 (7.6 m; 4575 m³/s), 1861
206 which ranked between 7m (4100 m³/s) and 8.2 m (5600 m³/s), 1890 (7.1 m; 4260 m³/s), 1846
207 and 1847 (7.0 m; 4135 m³/s). For the flood event of 9 September 2002, the gauge reading was
208 initially recorded as 7.60 m in the FWD survey, but a review led to it being adjusted to and
209 ultimately validated at 5.60 m with hydraulic modelling, as the initial reading proved
210 inconsistent with the high-water marks available in the vicinity. The interpretation adopted
211 jointly with the FFD is that the reading was taken upstream of the Anduze road bridge,
212 whereas the gauge is downstream. Given the very rough profile of the channel, the hydraulic
213 model yields an estimate of 3500 m³/s with a very large error interval [2590 ; 5870 m³/s]. It
214 should be noted that the value of 6180 m³/s that would have been obtained at Anduze (540
215 km²) at a flood crest of 7.60 m would also have been inconsistent from a hydrological
216 standpoint when compared with the discharge estimate made by the FFD further downstream
217 at Russans (1515 km²), which gave a range of 6000-6800 m³/s. The discharge interval used,
218 [2590, 5870 m³/s], agrees with other estimates performed by DDE (2003) and the engineering
219 firm ISL (2005), which range from 3000 and 3400 m³/s.

220

221 The flood of 9 September 2002 merits more detailed analysis because this event caused 23
222 deaths and an estimated €1.2 billion in damage (Huet *et al.*, 2003). In the upstream part of the
223 Gardon d'Anduze catchment, this flood is not listed as a major event, while that of 1958

224 remains the biggest since 1741. This is consistent with the rainfall pattern that caused the
225 2002 flood, which was characterised by very high accumulations on the intermediate part of
226 the catchment (Delrieu *et al.*, 2004), in contrast to the event of 1958, when the greatest
227 cumulative rainfall was located in the foothills of the Cévennes range, upstream from Anduze
228 (Jacquet, 1959). On the downstream part of the catchment, the flood is noteworthy for its
229 geographical scope and an epicentre of over 600 mm at Lédignan (Neppel *et al.*, 2003).
230 However, a paleohydrological analysis by Sheffer *et al.* (2008) in the canyons of the Gardon
231 shows that the 2002 flood level has been exceeded at least five times over the last 500 years,
232 based on sediment traces and dating of organic and mineral particles.

233

234

235 **III. FREQUENCY ANALYSIS OF FLOOD DATA**

236

237 The aim is to estimate flood quantiles from the samples collected for the recent and historical
238 periods. This estimate needs to take account of the fact that the data are incomplete and that
239 the discharge values are estimated using a hydraulic model and subject to considerable
240 uncertainty.

241 The estimation of flood quantiles can be based on data extracted from two distinct sampling
242 approaches. The peak-over-threshold (POT) approach uses flood peaks exceeding a
243 predefined threshold. Since the exhaustiveness of data from the historical period is related to a
244 perception threshold, it seems natural to use a POT approach, with a first exceedance
245 threshold equal to the perception threshold during the historical period, and a second, lower,
246 exceedance threshold during the systematic period. An example of POT-analysis of historical
247 data can be found in the paper by Parent and Bernier (2003). Alternatively, historical data can
248 also be included in the analysis of annual maxima (AM, see e.g. Naulet *et al.*, 2006). The

249 perception threshold is considered as a censoring threshold in this case. In this study, we
250 opted for the AM approach.

251 The pros and cons of each approach for analyzing historical data are still unclear. An obvious
252 drawback of the AM approach would be the loss of data if two (or more) floods happened to
253 exceed the perception threshold within the same year. However, this is unlikely to occur with
254 high perception thresholds. In particular, this did not occur in the dataset studied in this paper.
255 A formal evaluation of the relative merits of the AM and POT approaches for analysing
256 historical data would be of great interest; however, it is considered to lie beyond the scope of
257 the present paper and is left for future work.

258 Let X_t be the random variable representing the “true” annual maximum discharge at the
259 gauging station for year t ($t = 1, \dots, T$). Extreme value theory suggests using a generalized
260 extreme value (GEV) distribution to model such data (e.g., Embrecht *et al.*, 1997). The
261 probability density function f (pdf) and the cumulative density function F (cdf) of a
262 $GEV(\mu, \lambda, \xi)$, where μ , λ and ξ are respectively the location, scale and shape parameters, are
263 given by:

264

$$f(x | \mu, \lambda, \xi) = (1/\lambda) [1 - \xi(x - \mu)/\lambda]^{1/\xi - 1} \exp\left\{-[1 - \xi(x - \mu)/\lambda]^{1/\xi}\right\} \quad (1)$$

$$F(x | \mu, \lambda, \xi) = \exp\left\{-[1 - \xi(x - \mu)/\lambda]^{1/\xi}\right\}$$

$$\lambda > 0; \xi \neq 0; 1 - \xi(x - \mu)/\lambda > 0$$

265

266 The case $\xi = 0$ corresponds to the Gumbel distribution, and is equal to the limit of equation

267 (1) when $\xi \rightarrow 0$:

268

$$f(x | \mu, \lambda) = (1 / \lambda) \exp \left\{ -\frac{(x - \mu)}{\lambda} - \exp \left(-\frac{(x - \mu)}{\lambda} \right) \right\} \quad (2)$$

$$F(x | \mu, \lambda) = \exp \left\{ -\exp \left(-\frac{(x - \mu)}{\lambda} \right) \right\}$$

$$\lambda > 0$$

269

270 The main task of frequency analysis is to estimate the parameter vector $\theta = (\mu, \lambda, \xi)$. A
 271 Bayesian approach is used in this paper (e.g., Gelman et al., 1995). Standard frequency
 272 analyses usually neglect the possible errors corrupting observed data. In this case, the
 273 posterior distribution $p(\theta|X)$ is simply obtained by combining prior information on the
 274 distribution of the parameters $p(\theta)$ and the likelihood of the observations vector $X=(X_t)_{t=1, \dots, n}$,
 275 written as $p(X|\theta)$:

276

$$p(\theta|X) = \frac{p(X|\theta)p(\theta)}{\int p(X|\theta)p(\theta)d\theta} \propto p(X|\theta)p(\theta) \quad (3)$$

277 where the symbol ‘ \propto ’ denotes proportionality.

278

279 1. Error model

280 Unfortunately, the assumption that observed runoff data are error-free is untenable in most
 281 applications involving historical data. An error model linking the “true” runoff X_t (which is
 282 unknown, but whose distribution is wanted) with the “observed” runoff \tilde{X}_t (derived from a
 283 hydraulic model) is needed. Further notation needs to be defined for this purpose.

284 Let H_t be the “true” water level reached during the highest flood of year t , and \tilde{H}_t the
 285 corresponding observed level. When the historical information collected is deemed accurate
 286 enough, or for data in the systematic measurement period, the error affecting observed water
 287 level may be neglected, leading to the assumption $H_t = \tilde{H}_t$. However, incomplete information

288 may lead to relax this assumption, by simply assuming the true level is contained in an
289 interval. This can be formalized as follows:

$$H_t = \tilde{H}_t + \delta_t, \delta_t \in [-l_t; l_t] \quad (4)$$

290 Using the above convention, the observed level \tilde{H}_t is the centre of the interval of length $2l_t$.
291 Importantly, it will be assumed that the errors δ_t are independent from year to year. The
292 rationale behind this assumption is that such errors are due to incompleteness or inconsistency
293 of the historical information. The error made at year t should therefore not impact the error at
294 year $t+1$, since it only depends on the availability and consistency of historical information.
295 Runoff data are then derived by applying the rating curve obtained from the hydraulic model
296 to the observed levels. Since several rating curves may be used, let $\hat{\psi}_k(h)$ denote the k th
297 rating curve ($k = 1, \dots, N_c$). $\hat{\psi}_k(h)$ is an approximation of the “true” rating curve $\psi(h)$ linking
298 the true runoff with the true water level. The following error model will be used to describe
299 the error made during this approximation:

$$\psi(h) = \gamma_k \hat{\psi}_k(h) \quad (5)$$

300 This multiplicative error model is justified by the common observation that absolute rating
301 curve errors (differences between true and estimated discharges) increase with the discharge
302 value (e.g., Thyer et al., 2009; Reitan and Petersen-Overleir, 2009). Contrarily to water level
303 errors, the rating curve error is systematic, i.e. all runoff data included in the period of validity
304 of the k th rating curve are affected by the same multiplicative error γ_k . This error model is a
305 particular case of the rating curve error model proposed by Kuczera (1996).
306 Combining equations (4) and (5) allows deriving the relationship between true and observed
307 runoff as follows:

$$\begin{aligned}
 X_t &= \psi(H_t) & (6) \\
 &= \gamma_k \hat{\psi}_k(H_t) \\
 &= \gamma_k \hat{\psi}_k(\tilde{H}_t + \delta_t) \\
 &= \gamma_k \left[\hat{\psi}_k(\tilde{H}_t) + \hat{\psi}_k(\tilde{H}_t + \delta_t) - \hat{\psi}_k(\tilde{H}_t) \right] \\
 &= \gamma_k \left[\tilde{X}_t^{(k)} + \hat{\psi}_k(\tilde{H}_t + \delta_t) - \hat{\psi}_k(\tilde{H}_t) \right] \\
 &= \gamma_k \left[\tilde{X}_t^{(k)} + \varepsilon_t \right], \\
 &\text{with } \varepsilon_t = \hat{\psi}_k(\tilde{H}_t + \delta_t) - \hat{\psi}_k(\tilde{H}_t)
 \end{aligned}$$

308 The superscript (k) has been introduced to recall the rating curve used to derive the observed
 309 runoff $\tilde{X}_t^{(k)}$. Since the additive water level error δ_t is included in the interval $[-l_t; l_t]$, the
 310 resulting additive runoff error ε_t is included in the interval
 311 $[\hat{\psi}_k(\tilde{H}_t - l_t) - \hat{\psi}_k(\tilde{H}_t); \hat{\psi}_k(\tilde{H}_t + l_t) - \hat{\psi}_k(\tilde{H}_t)] = [a_t; b_t]$.

312 The error model in equation (6) shows that observed runoff is affected by two different types
 313 of errors: a multiplicative systematic error stemming from the estimated rating curve, and
 314 independent event-specific errors stemming from the imperfect knowledge of the water level
 315 reached during historical floods.

316

317 2. Parameter estimation

318 In order to perform the Bayesian estimation of the GEV parameters, the likelihood of the
 319 observations $\tilde{X}_t^{(k)}$ needs to be derived. In a first step, inverting equation (6) gives the
 320 following relationship:

321

$$\tilde{X}_t^{(k)} = X_t / \gamma_k - \varepsilon_t \quad (7)$$

322 It is then possible to demonstrate that $p(\tilde{X}_t^{(k)} | \mu, \lambda, \xi, \gamma_k, \varepsilon_t)$, the distribution of an
 323 observation $\tilde{X}_t^{(k)}$, conditionally on errors γ_k and ε_t , is a $GEV(\mu / \gamma_k - \varepsilon_t, \lambda / \gamma_k, \xi)$ (see
 324 appendix 1).

325 The explicit treatment of errors leads to the introduction of additional unknown terms in the
 326 inference, namely vectors $\boldsymbol{\gamma}=(\gamma_1,\dots,\gamma_{Nc})$ and $\boldsymbol{\varepsilon}=(\varepsilon_1,\dots,\varepsilon_T)$. The length of vector $\boldsymbol{\gamma}$ is equal to the
 327 number of rating curves Nc used to reconstruct past discharges, which is likely to remain
 328 relatively small. However, the length of vector $\boldsymbol{\varepsilon}$ can theoretically be equal to the total number
 329 of years included in the analysis T . In practice, some components of $\boldsymbol{\varepsilon}$ can be fixed to zero,
 330 corresponding to flood events whose water levels are assumed to be known without any error
 331 (circles in Figure 2).

332 There are two options for treating these additional unknown terms: they can be included in the
 333 list of parameters to be estimated, or alternatively, they can be integrated out from the
 334 conditional distribution $p(\tilde{X}_t^{(k)} | \mu, \lambda, \xi, \gamma_k, \varepsilon_t)$ prior to the inference (e.g., *Kuczera, 1992*). In
 335 this paper, a mixed approach is adopted: parameter vector $\boldsymbol{\gamma}$ is included in the inference, but $\boldsymbol{\varepsilon}$
 336 is integrated out as follows:

$$p(\tilde{X}_t^{(k)} | \mu, \lambda, \xi, \gamma_k) = \int p(\tilde{X}_t^{(k)} | \mu, \lambda, \xi, \gamma_k, \varepsilon_t) p(\varepsilon_t) d\varepsilon_t \quad (8)$$

337 Applying equation (8) requires defining a prior probability distribution for the error term ε_t .
 338 Since ε_t is assumed to be included in the interval $[a_t; b_t]$, a natural choice is to use the uniform
 339 distribution on this interval. This choice is particularly interesting because it allows
 340 performing the integration in equation (8) analytically (see appendix 2). Under this
 341 assumption, the distribution of an observation $\tilde{X}_t^{(k)}$, conditionally on errors γ_k only, is given
 342 by:

$$p(\tilde{X}_t^{(k)} | \mu, \lambda, \xi, \gamma_k) = \frac{1}{b_t - a_t} \left[F(\tilde{x}_t^{(k)} + b_t | \mu / \gamma_k, \lambda / \gamma_k, \xi) - F(\tilde{x}_t^{(k)} + a_t | \mu / \gamma_k, \lambda / \gamma_k, \xi) \right] \quad (9)$$

343 Note that in the particular case where ε_t is forced to zero (no water-level-related error), the
 344 conditional distribution $p(\tilde{X}_t^{(k)} | \mu, \lambda, \xi, \gamma_k)$ is simply given by:

$$p(\tilde{X}_t^{(k)} | \mu, \lambda, \xi, \gamma_k) = f(\tilde{x}_t^{(k)} | \mu / \gamma_k, \lambda / \gamma_k, \xi) \quad (10)$$

345 which appears to be the limit of the right hand side of equation (9) when $a_t \rightarrow b_t$.
 346 Equations (9) and (10) can then be used to derive the likelihood function of the whole set of
 347 observations \mathbf{X} . For a given rating curve (k), let S_k be the set of years included in the period of
 348 validity of the rating curve for which an observation is available (either with point or interval
 349 water level data, corresponding to circles and intervals in figure 2). Let us further assume that
 350 n_k years correspond to censored data, i.e. the only available information is that the annual
 351 maximum flood did not exceed the perception threshold u_k . Lastly, it is assumed that annual
 352 maxima are independent and identically distributed. Under these assumptions, following Reis
 353 and Stedinger (2005), the likelihood function is proportional to:

$$p(\mathbf{X} | \mu, \lambda, \xi, \gamma) \propto \prod_{k=1, Nc} \left[\prod_{t \in S_k} \{ p(\tilde{X}_t^{(k)} | \mu, \lambda, \xi, \gamma_k) \} \right] [F(u_k | \mu / \gamma_k, \lambda / \gamma_k, \xi)]^{n_k} \quad (11)$$

354 In equation (11), the term $F(u_k | \mu / \gamma_k, \lambda / \gamma_k, \xi)$ is the cdf of the GEV distribution evaluated
 355 at the perception threshold, and corresponds to the contribution of a censored data (i.e. below
 356 the threshold) to the likelihood. The term $p(\tilde{X}_t^{(k)} | \mu, \lambda, \xi, \gamma_k)$ corresponds to the contribution
 357 of an observation to the likelihood. It is evaluated with equation (9) or (10) for interval or
 358 point data, respectively.

359 Assuming prior independence, the posterior pdf can then be derived (up to a constant of
 360 proportionality) as follows:

$$\begin{aligned} p(\mu, \lambda, \xi, \gamma | \mathbf{X}) &\propto p(\mathbf{X} | \mu, \lambda, \xi, \gamma) p(\mu, \lambda, \xi, \gamma) \\ &\propto p(\mathbf{X} | \mu, \lambda, \xi, \gamma) p(\mu) p(\lambda) p(\xi) \prod_{k=1, Nc} p(\gamma_k) \end{aligned} \quad (12)$$

361 In this case study, the joint prior distribution of the three GEV parameters is obtained by
 362 assuming their prior independence and by using very broad, uniform distributions for location
 363 (μ) and scale (λ) parameters. For the shape parameter ξ , we use a Gaussian distribution
 364 centred on zero with a standard deviation of 0.3, which means that the interval $[-0.6 ; 0.6]$

365 contains over 90% of the prior density. Such a prior distribution for the shape parameter is
366 similar to the “geophysical prior” of Martins and Stedinger (2000). Thus:

$$p(\mu, \lambda, \xi) = U(\mu | -10000, 10000) U(\lambda | 0, 10000) N(\xi | 0, 0.3^2) \quad (13)$$

367 The assumption of prior independence is mainly used here for convenience. However, since
368 flat priors are used for the location and scale parameters in order to reflect the lack of prior
369 knowledge on these parameters, it seems natural not to introduce any form of dependence
370 between them. Importantly, prior independence does not imply that the parameter posterior
371 distributions will be independent (i.e., the parameter estimates might be dependent).
372 Moreover, methods for specifying an informative prior distribution (without necessarily using
373 the assumption of prior independence) have been proposed (e.g. Coles and Powell, 1996;
374 Renard et al., 2006a; Ribatet et al., 2006) and could be used within this inference framework.

375
376 The prior distributions of rating curve error parameters γ remains to be specified. This can be
377 done using the results of the hydraulic sensitivity study (Figure 5). More accurately, a
378 triangular prior distribution is used (Figure 6). The mode of this distribution is obtained for
379 $\gamma=1$ (no error), while the base expands between values *min* and *max*. These values are
380 determined so that the corresponding rating curves (thick lines in figure 4) roughly match the
381 limits given by the hydraulic sensitivity analysis. In this case study, these values [*min*;*max*]
382 are equal to [0.8;1.3] for the historical rating curve and [0.8;1.25] for the recent rating curve.
383 Note that the choice of such a triangular distribution is somewhat arbitrary. Alternative
384 assumptions may be used (e.g. O'Connel, 2005; O'Connel, et al., 2002). However, this choice
385 is a delicate issue, since a hydraulic sensitivity analysis does not provide the full distribution
386 of the rating curve error. This would require a more in-depth probabilistic assessment of the
387 propagation of errors in the hydraulic model. This is considered to lie beyond the scope of this
388 paper and is left for future work.

389

390 Lastly, Markov chain Monte Carlo (MCMC) algorithms are applied to the posterior
391 distribution (12), making it possible to estimate the parameters and derived quantities,
392 including flood quantiles. We used the two-stage MCMC strategy proposed by Renard *et al.*
393 (2006b) . We refer to this paper for a detailed description of the algorithms used. Shortly, the
394 first stage of the algorithm is an adaptive Gibbs sampler (Geman and Geman, 1984), which is
395 used to perform a preliminary exploration of the posterior distribution properties (notably in
396 terms of posterior covariance). In a second step, a standard Metropolis sampler (Metropolis
397 and Ulam, 1949; Metropolis et al., 1953) is used, with a Gaussian jump distribution whose
398 covariance matrix is specified using the preliminary exploration performed at stage one. The
399 Metropolis sampler is ran during 100,000 iterations, with the first half of the iterations being
400 considered as a burn-in period and being therefore discarded. Convergence was assessed by
401 evolving four parallel chains and verifying that the Gelman-Rubin criteria (Gelman et al.,
402 1995) were close to one for all inferred quantities.

403

404 **3. Results**

405

406 The modelled series (Figure 2) stems from two information sources: i) data from the flood
407 warning gauge at Anduze (1892-2005), and ii) data from the historical survey, covering the
408 1741-1891 period. The systematic period is exceptionally long at this site, lasting over 100
409 years. Over the historical period, the perception threshold was taken to be 2961 m³/s,
410 corresponding to the station's alert level. It should be remembered that discharge values are
411 reconstructed on the basis of one recent (post-1985) and one historical (pre-1985) rating
412 curve.

413

414 In a first step, the posterior distribution of GEV parameters obtained with the whole dataset
415 (1741-2005) is evaluated. Figure 7 compares the posterior pdfs obtained when
416 systematic/independent errors are accounted for (thick black lines) or ignored (thin grey
417 lines). It shows that the location and scale parameters estimates are highly sensitive to the
418 treatment of errors affecting data. Conversely, the shape parameter remains similar: this can
419 be explained by the fact that the shape parameters of observed and true runoffs are identical
420 (see appendix 1) with the error model (7) assumed in this study. The posterior pdfs of the
421 multiplicative error terms γ_1 and γ_2 contain the value 1: the probabilistic model identifies no
422 systematic rating curve error.

423 In a second step, the impact of additional historical information is evaluated by comparing
424 quantiles obtained using the 1892-2005 data with quantiles obtained using the whole 1741-
425 2005 dataset (Figure 8). Note that the treatment of systematic/independent errors is identical
426 in both cases, with all errors being accounted for. Using historical data (pre-1892) appreciably
427 changes the estimated quantiles, owing to the presence of many events in the vicinity of 4000
428 m^3/s . The fit with empirical frequencies is not very satisfactory, but given the shape suggested
429 by these empirical frequencies, it seems likely that no curve would fit these points
430 convincingly.

431

432 **4. Sensitivity analysis**

433

434 Section 3 illustrated the impact of errors affecting discharge estimates when historical
435 information is included in the inference. In this analysis, several quantities are fixed prior to
436 the inference: (i) the width of the triangular prior (Figure 6) for systematic rating curve errors;
437 (ii) the width of the discharge uncertainty intervals due to independent errors affecting water
438 levels (intervals in figure 2); (iii) the value of the perception threshold. A sensitivity analysis

439 is carried out in this section to evaluate whether modifications of these predefined quantities
440 significantly impact the estimated quantiles.

441

442 Sensitivity to the triangular prior for rating curve errors is studied by increasing/decreasing
443 the width of the triangle base. More precisely, the original triangle with base $[a;b]$ is replaced
444 by a triangle with base $[a';b']$ defined by:

445

$$\begin{aligned} a' &= a - z(1 - a) \\ b' &= b + z(b - 1) \end{aligned} \tag{14}$$

446

447 z corresponds to an inflation factor. When $z = 0$, the interval $[a;b]$ is unchanged; when $z = 1$,
448 the width of the interval is doubled; when $z = -1$, the interval collapses to the single point 1.
449 The latter case yields a Dirac prior distribution, which corresponds to ignoring the rating
450 curve systematic error.

451 Sensitivity to the intervals describing independent discharge errors (ε_i , equation (6)) makes
452 use of a similar inflation factor, except that the value 1 in equation (14) is replaced by the
453 centre of the interval $[a;b]$:

454

$$\begin{aligned} a' &= a - z((a + b)/2 - a) \\ b' &= b + z(b - (a + b)/2) \end{aligned} \tag{15}$$

455

456 Lastly, the sensitivity to the choice of the perception threshold u is studied by
457 increasing/decreasing the value of u . When u is decreased, the historical information is
458 preserved but its exhaustiveness occurs for a lower discharge. In some sense, decreasing the
459 perception threshold therefore tests the robustness of the inference when the exhaustiveness

460 assessment is unduly optimistic. Conversely, when u is increased, all historical floods
461 becoming smaller than u are discarded from the analysis.

462

463 Results from the sensitivity analysis are shown in figure 9 and yield interesting observations:

464 (i) The prior for rating curve systematic errors exerts a significant influence on the
465 estimated quantiles. In particular, the uncertainty strongly increases with the prior
466 width. This demonstrates the influence of the chosen prior distributions on the
467 estimates, and calls for further research to derive meaningful priors from the
468 hydraulic analysis.

469 (ii) Independent discharge errors stemming from imprecise knowledge of the water
470 levels appear to impact the results to a lesser extent. In particular, ignoring these
471 errors ($z = -1$) leaves the original estimated quantiles ($z = 0$) almost unchanged.

472 (iii) The choice of the perception threshold also exerts a significant influence on the
473 inference, with the estimated quantiles being impacted by both increases and
474 decreases of the threshold. As expected, the inference using historical information
475 becomes similar to the inference solely using the data from the recent period when
476 the threshold reaches high levels ($u = 5,000$ or $10,000 \text{ m}^3 \cdot \text{s}^{-1}$).

477

478 Although interesting, these observations should not be extrapolated beyond this particular
479 case study. In particular, the relative influence of systematic and independent errors might be
480 case-specific. This will be established in future work.

481

482 **IV DISCUSSION**

483

484 The approach detailed for the Anduze catchment was also applied to the other four
485 catchments of the Gard river listed in section 2. For all of these catchments, the following
486 conclusions may be drawn. First, the use of historical data shows that Frechet-type
487 distributions seem to represent flood discharge distributions better than the Gumbel
488 distribution. For these catchments, the posterior distributions of the shape coefficient indicate
489 that the coefficients are significantly different from zero, ranging from -0.25 at Alès to -0.5 at
490 Anduze. The high values of the shape coefficient for the two main tributaries of the Gardon
491 d'Anduze (Mialet and St-Jean) are consistent with the estimates at Anduze. We reach here the
492 same conclusions as those obtained by Naulet *et al.* (2005) for the Ardèche river and
493 Payrastre *et al.* (2005) for four catchments of the Aude river system. Thus, even when the
494 systematic period is exceptionally long – over 100 years – the distributions of discharge
495 values are clearly modified when historical floods are taken into account. Table 1 presents the
496 estimates of the 10-year and 100-year quantiles for the four catchments with their respective
497 confidence intervals. It can be seen that the ratio of the 100-year quantiles for the historical
498 period to those for the systematic period ranges from 1.1 for the Gardon de Mialet to 1.85 for
499 the Gardon d'Anduze at Anduze. This indicates once again the importance of taking historical
500 flood data into consideration in the predetermination of flood volumes, even when long
501 systematic time series are available.

502

503 Examination of the confidence intervals of the quantiles shows that, in contrast to what one
504 might expect, these intervals can become wider when historical floods are taken into account
505 compared to the systematic period alone. This result may be due to the high level of
506 uncertainty affecting the highest historical floods and to the model used for systematic errors.

507

508 The specific 100-year flood discharge values obtained when the historical period is used
509 range from 5 to 10 m³/s/km², a standard order of magnitude for Mediterranean catchments.
510 More specifically, we tried to compare our estimates of 100-year flood discharge (Q100) with
511 other approaches (Table 2). The empirical relationships established for the Gard region by
512 Bressand and Golosof (1996) give:

513

$$Q_{\text{rare}} = 30 A^{0.75} \quad \text{and} \quad Q_{\text{exc.}} = 50 A^{0.75} \quad (13)$$

514

515 where Q_{rare} and $Q_{\text{exc.}}$ give orders of magnitude for 100-year and 1000-year flood discharge
516 respectively, for a catchment with a surface area A .

517

518 Our estimates of Q100 using the historical data lie in an interval of -30% to +50% with
519 respect to Q_{rare} . The historical 100-year flood discharge is higher than these estimates for the
520 Anduze and Saint-Jean du Gard catchments. In addition, except in the case of the Gardon
521 d'Anduze, these specific 100-year discharge values are below the highest regional curves of
522 specific discharge values Q_{max} from major floods in Europe, constructed by Stanescu (2004)
523 from a database of more than 700 flood events.

524 The specific discharge estimate of Q100 issued from a regional stochastic rainfall generator
525 mixed with a rainfall-runoff model (Arnaud *et al.*, 2007), called Shyreg model, presents less
526 variations among the four catchments. It seems more logical as the four basins have similar
527 climatic and morphometric characteristics. Q100 estimates at Ales and Mialet are similar, as
528 large differences between historical and Shyreg approaches are observed at St Jean (9,6
529 versus 6,4) and especially at Anduze (9,5 versus 3,8). Large uncertainties on discharge
530 estimates could explain such differences. Additional studies, based on both historical and

531 regional approaches, are needed to better understand the advantages and limits of each kind of
532 information.

533

534 **V CONCLUSIONS**

535

536 A three-step procedure has been used to estimate discharge from major floods on the various
537 Gardon catchments.

538

539 First, a historical survey identified and collected data on historical floods. The recent period is
540 particularly rich in information on the studied catchments: the archives of daily discharge
541 readings preserved by the flood forecasting department (FFD) allowed us to reconstruct the
542 time series back to 1892, when the FFD was created. Information in the archives of the Gard
543 region allowed us to supplement the Anduze time series with 29 unindexed flood events that
544 occurred between 1741 and 1891. In view of this research, we can guarantee that the sample
545 is complete for all floods since 1741 that exceeded the 1892 alert level.

546

547 These data were then used to reconstruct flood discharge series and their uncertainty, based on
548 a hydraulic model. Several models were constructed for each site in order to take account, to
549 the extent possible, of geomorphological changes in the riverbeds and changes in flood
550 gauges during the period analysed. Recent and historical rating curves were constructed. For a
551 given water level reading, they output a central discharge value with an uncertainty interval
552 that takes account of the roughness of the channel in the reach considered. When this is
553 cumulated with the uncertainty affecting water level readings, the overall uncertainty for the
554 largest floods can be very high, with the relative error of the reconstructed discharge values
555 reaching 100% in some cases.

556

557 Lastly, a Bayesian frequency analysis is performed in order to analyze the sample of recent
558 and historical maxima, accounting for additive and multiplicative error affecting discharge
559 values, respectively due to random error in water level readings and systematic rating curve
560 error.

561

562 The use of historical flood data yielded mixed results. It lengthens the study period, but the
563 reconstructed discharge values are in some cases subject to very high uncertainty, which is
564 due among other things to the rating curves and affects recent discharge values as well. This
565 demonstrates the need to improve discharge measurement, notably by increasing the number
566 of flood gauges, so as to reduce the sources of uncertainty, at least for recent discharge values.
567 When this uncertainty affecting discharge is taken into account in the probabilistic model, the
568 confidence intervals for quantiles are in some cases higher when historical flood data are used
569 than when the analysis is based solely on the recent discharge series. This demonstrates the
570 need for careful evaluation of the various sources of uncertainty in order to assess the impact
571 of using historical flood data and for their integration in the probabilistic model. In addition,
572 the historical quantiles have been found of the same order of magnitude as those obtained
573 through regional empirical methods, for two of the four studied catchments.

574

575

575 **Appendix 1**

576 The aim is to derive the distribution of $\tilde{X}_t^{(k)} = X_t / \gamma_k - \varepsilon_t$, conditionally on errors γ_k and ε_t .

577 For this purpose, let us write the cdf of $\tilde{X}_t^{(k)}$ at a given value x :

$$\begin{aligned} \Pr(\tilde{X}_t^{(k)} \leq x) &= \Pr(X_t / \gamma_k - \varepsilon_t \leq x) \\ &= \Pr(X_t \leq \gamma_k(x + \varepsilon_t)) \end{aligned} \quad (16)$$

578 Since $X_t \sim GEV(\mu, \lambda, \xi)$, equation (1) yields:

$$\begin{aligned} \Pr(\tilde{X}_t^{(k)} \leq x) &= \Pr(X_t \leq \gamma_k(x + \varepsilon_t)) \\ &= \exp\left\{-\left[1 - \xi(\gamma_k(x + \varepsilon_t) - \mu) / \lambda\right]^{1/\xi}\right\} \\ &= \exp\left\{-\left[1 - \gamma_k \xi(x + \varepsilon_t - \mu / \gamma_k) / \lambda\right]^{1/\xi}\right\} \\ &= \exp\left\{-\left[1 - \xi(x - (\mu / \gamma_k - \varepsilon_t)) / (\lambda / \gamma_k)\right]^{1/\xi}\right\} \end{aligned} \quad (17)$$

579 The latter expression is equal to the cdf of a $GEV(\mu / \gamma_k - \varepsilon_t, \lambda / \gamma_k, \xi)$ evaluated at x .

580

581 **Appendix 2**

582 The aim is to perform the following integration:

$$p(\tilde{X}_t^{(k)} | \mu, \lambda, \xi, \gamma_k) = \int p(\tilde{X}_t^{(k)} | \mu, \lambda, \xi, \gamma_k, \varepsilon_t) p(\varepsilon_t) d\varepsilon_t \quad (18)$$

583 Assuming $p(\varepsilon_t)$ is a uniform distribution on $[a_t, b_t]$ yields:

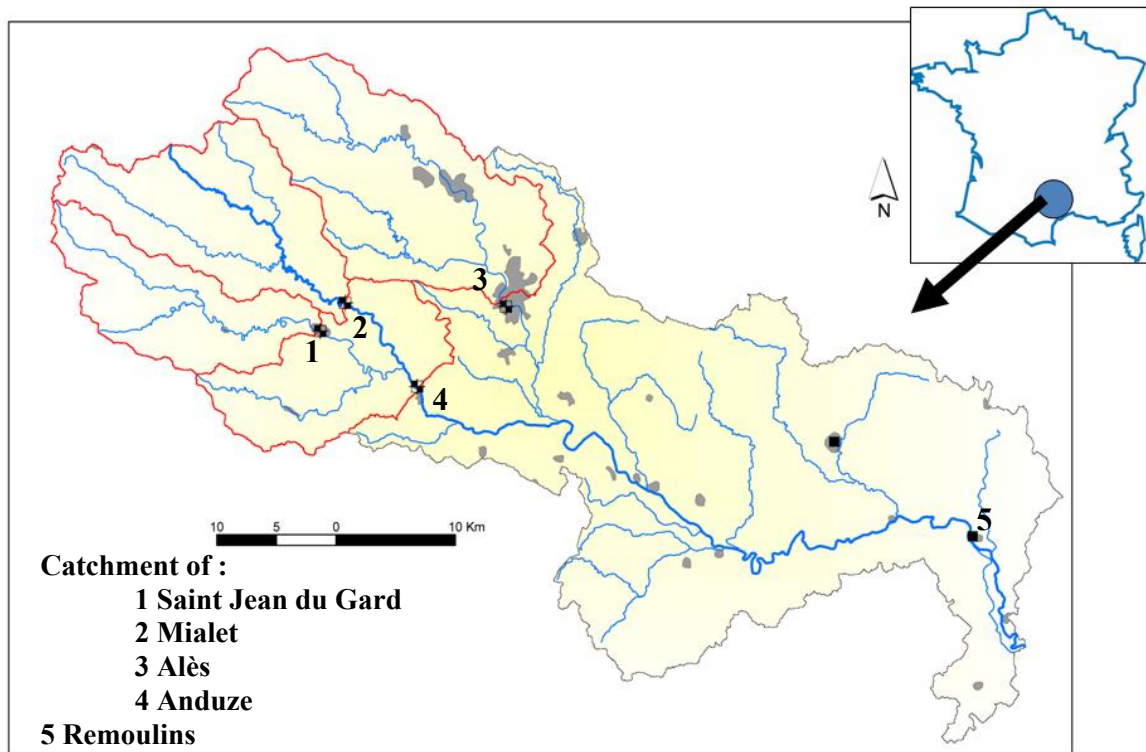
$$\begin{aligned} p(\tilde{X}_t^{(k)} | \mu, \lambda, \xi, \gamma_k) & \\ &= \int_{a_t}^{b_t} f(\tilde{x}_t^{(k)} | \mu / \gamma_k - \varepsilon_t, \lambda / \gamma_k, \xi) \frac{1}{b_t - a_t} d\varepsilon_t \\ &= \frac{1}{b_t - a_t} \int_{a_t}^{b_t} (\gamma_k / \lambda) \left[1 - \xi \gamma_k (\tilde{x}_t^{(k)} - \mu / \gamma_k + \varepsilon_t) / \lambda\right]^{\frac{1}{\xi} - 1} \exp\left\{-\left[1 - \xi \gamma_k (\tilde{x}_t^{(k)} - \mu / \gamma_k + \varepsilon_t) / \lambda\right]^{1/\xi}\right\} d\varepsilon_t \end{aligned} \quad (19)$$

584 Using the substitution $u = \tilde{x}_t^{(k)} + \varepsilon_t$:

$$\begin{aligned}
 & p(\tilde{X}_t^{(k)} \mid \mu, \lambda, \xi, \gamma_k) \tag{20} \\
 &= \frac{1}{b_t - a_t} \int_{\tilde{x}_t^{(k)} + a_t}^{\tilde{x}_t^{(k)} + b_t} (\gamma_k / \lambda) [1 - \xi \gamma_k (u - \mu / \gamma_k) / \lambda]^{\frac{1}{\xi} - 1} \exp \left\{ - [1 - \xi \gamma_k (u - \mu / \gamma_k) / \lambda]^{1/\xi} \right\} du \\
 &= \frac{1}{b_t - a_t} \int_{\tilde{x}_t^{(k)} + a_t}^{\tilde{x}_t^{(k)} + b_t} f(u \mid \mu / \gamma_k, \lambda / \gamma_k, \xi) du \\
 &= \frac{1}{b_t - a_t} \left[F(\tilde{x}_t^{(k)} + b_t \mid \mu / \gamma_k, \lambda / \gamma_k, \xi) - F(\tilde{x}_t^{(k)} + a_t \mid \mu / \gamma_k, \lambda / \gamma_k, \xi) \right]
 \end{aligned}$$

585

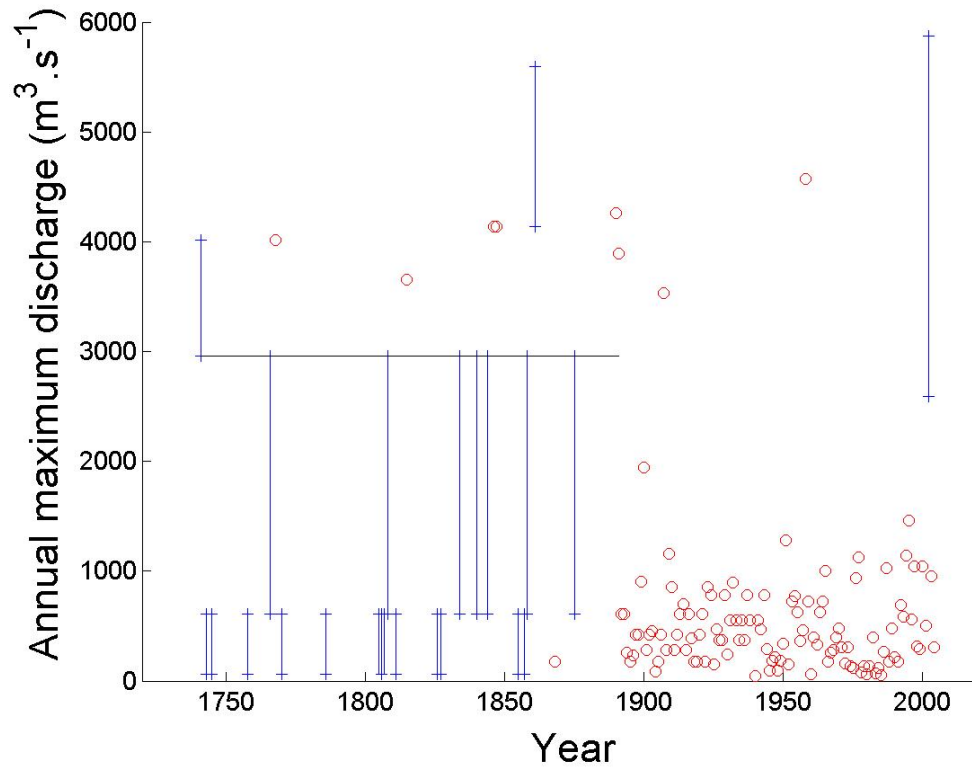
585



586

587 **Figure 1: Overview of the four studied catchments**

588

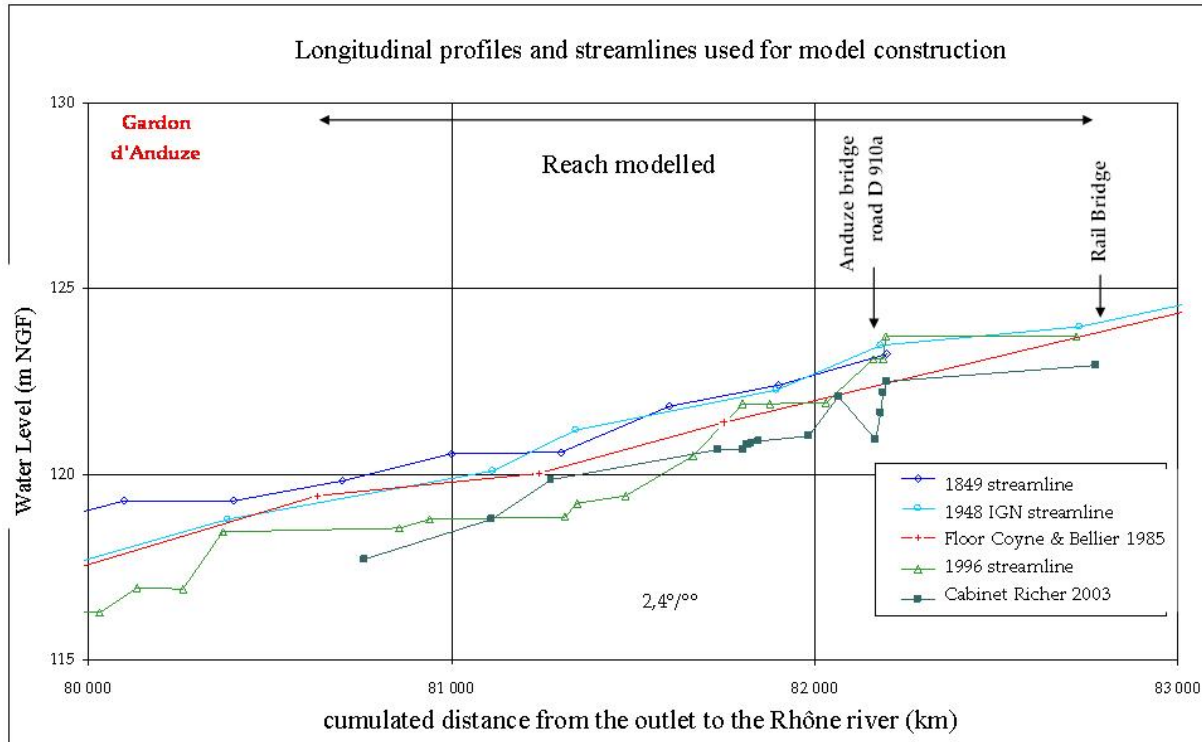


588

589 **Figure 2: Floods on the Gardon d'Anduze river at Anduze (1741-2005). Circles correspond to events**
590 **whose water level is known with high precision. Intervals represent the uncertainty due to imperfect**
591 **knowledge of the water level reached during the event. The horizontal line is the perception threshold.**

592

592

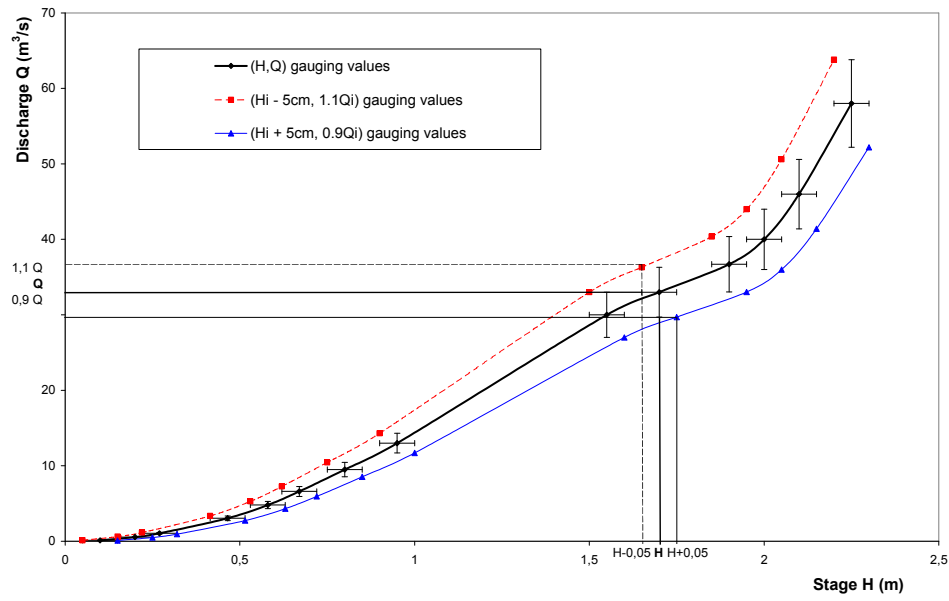


593

594 **Figure 3: Longitudinal profile of the Gardon d'Anduze river at Anduze**

595

596



597 **Figure 4: Envelope curves of the stage-discharge relationship**

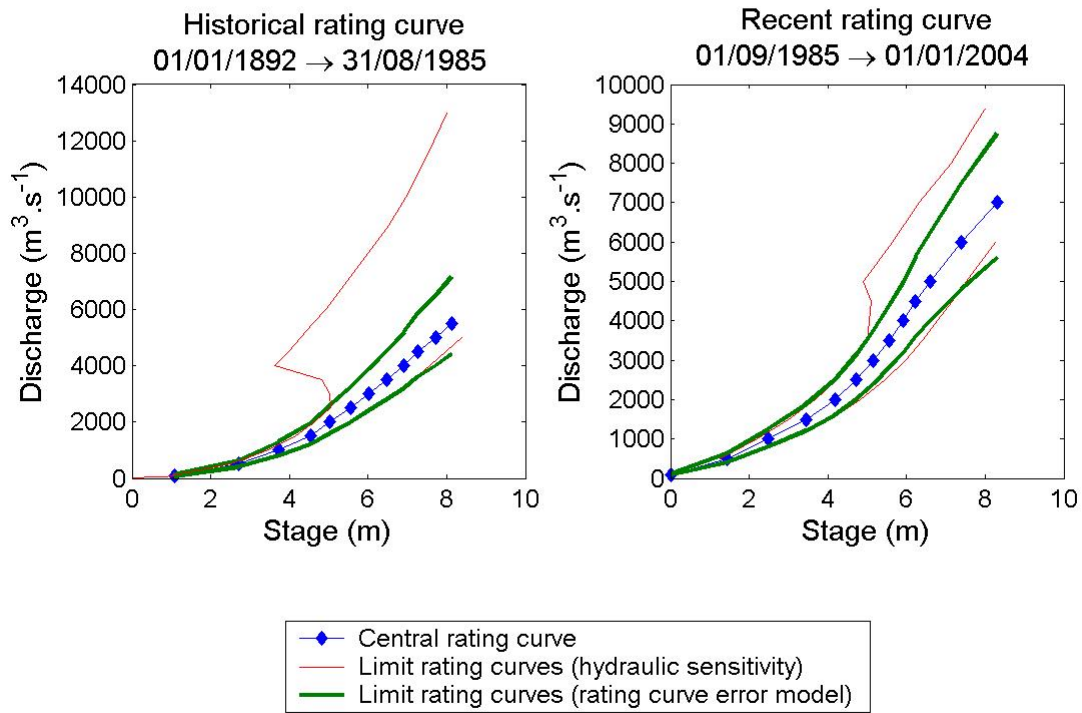
598

599

599

600

601



602

603

604 **Figure 5: Historical and recent rating curves**

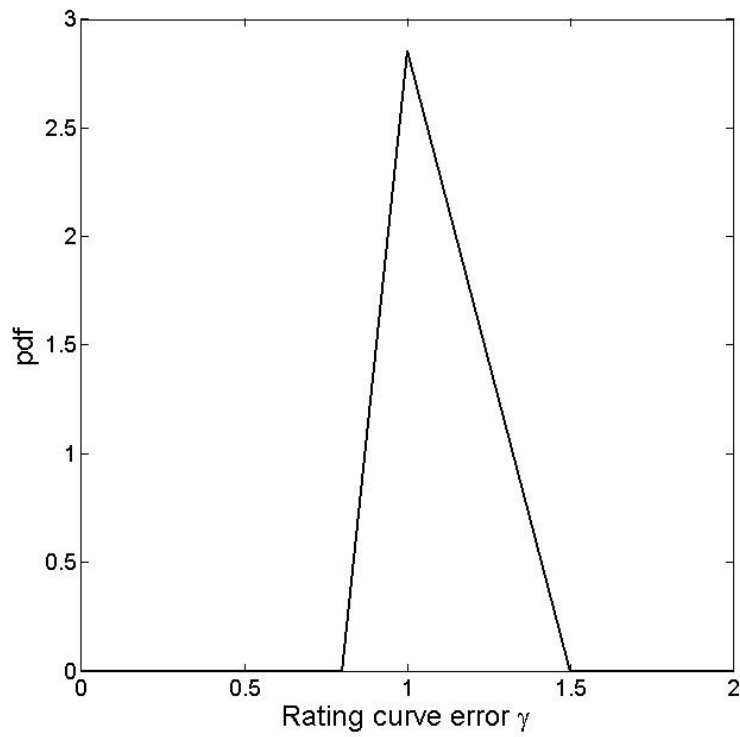
605

605

606

607

608



609

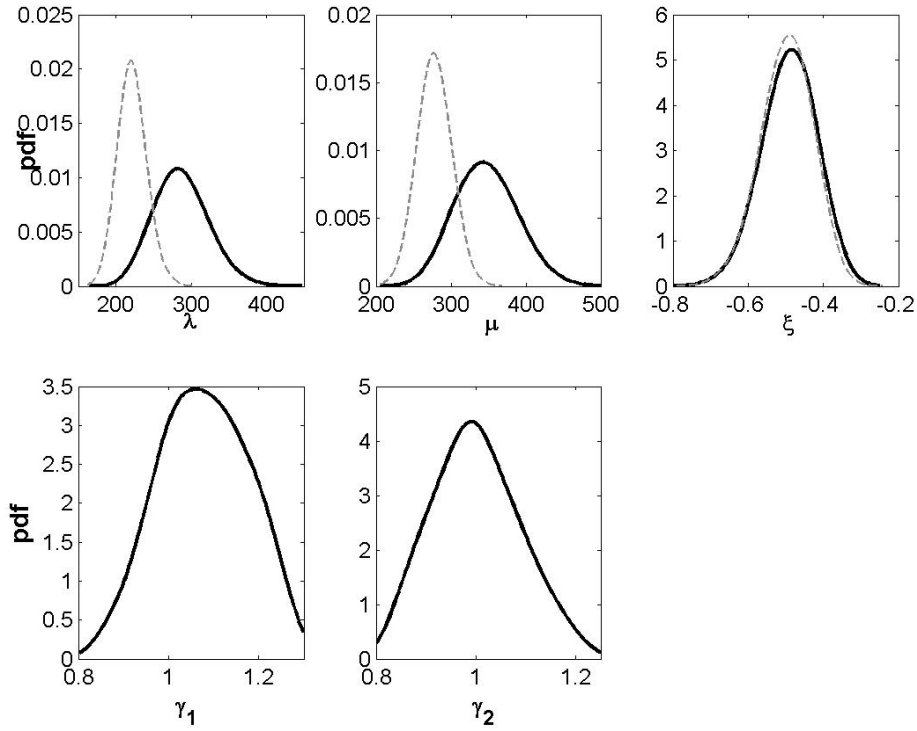
610

611 **Figure 6: Illustration of a triangular prior pdf for the rating curve error parameter γ**

612

612

613



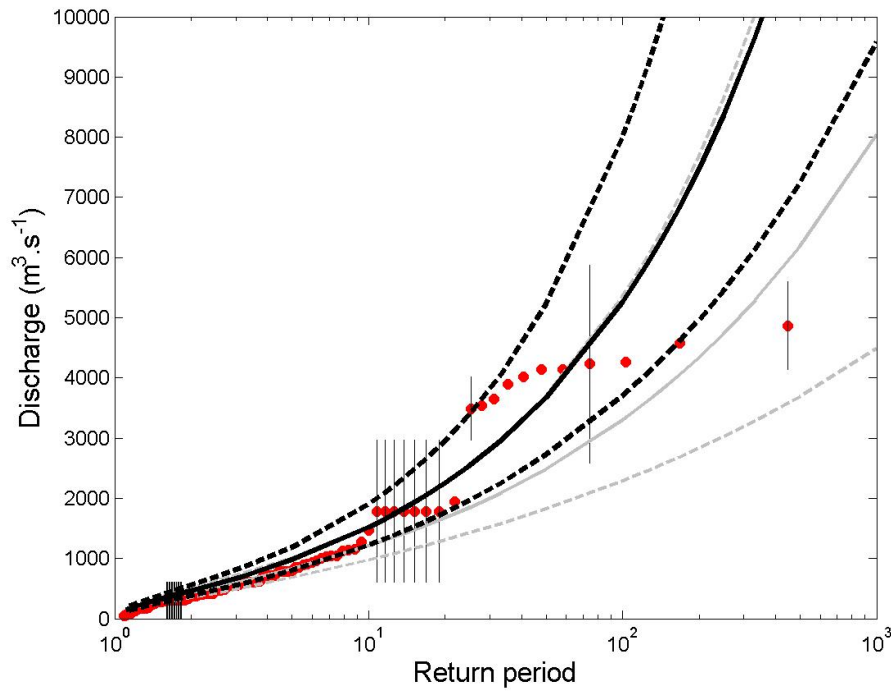
614

615 **Figure 7: Posterior pdfs of GEV parameters λ , μ , ξ , and of rating curve error parameters γ_1 and γ_2 ,**

616 **obtained with the whole dataset 1741-2005. Thick black lines = systematic and independent errors**

617 **accounted for; thin grey lines: systematic and independent errors ignored.**

618



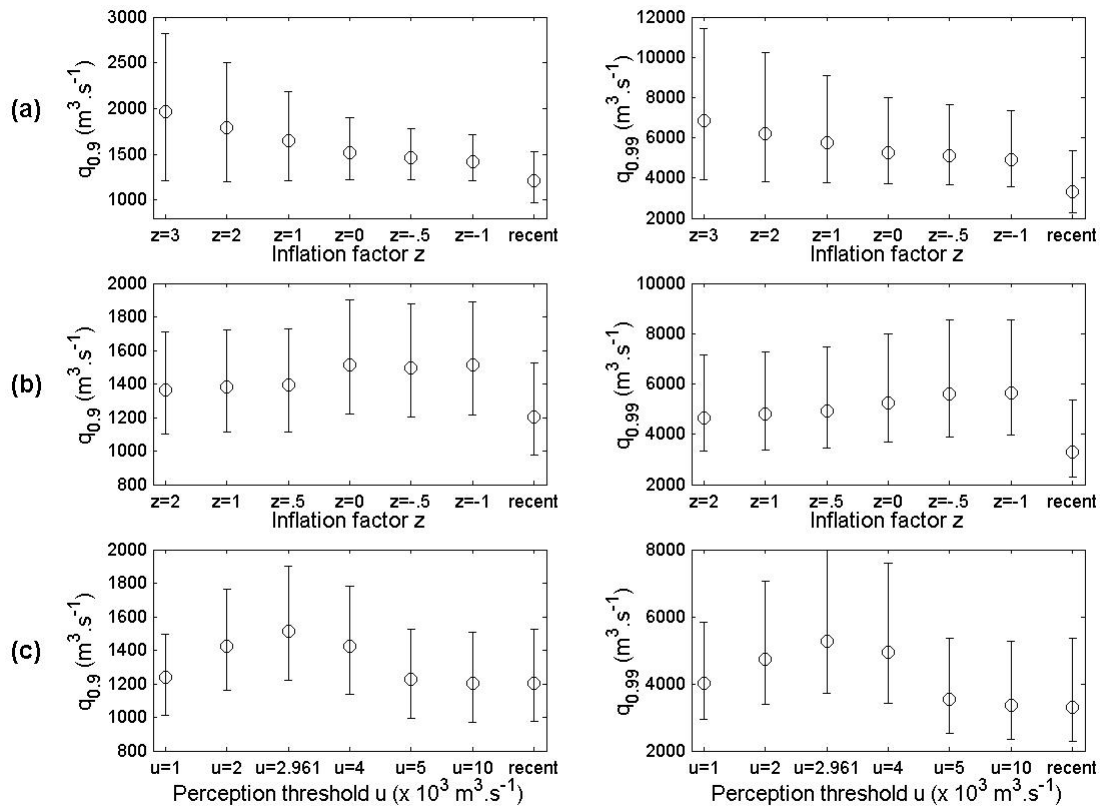
618

619 **Figure 8: GEV distribution of annual maxima at Anduze, with 90% posterior intervals**

620 Note: Thick lines = whole period (1741-2005); thin lines = the systematic period (1892-2005); circles =
621 empirical frequencies.

622

622



623

624 **Figure 9: Sensitivity of 0.9- and 0.99-quantiles posterior estimates. Circles represent posterior medians,**
 625 **bars represent 90% posterior intervals. (a) Sensitivity to the prior for systematic rating curve errors; (b)**
 626 **sensitivity to the width of intervals describing independent errors; (c) sensitivity to the perception**
 627 **threshold. ‘recent’ denotes results with data from the period 1892-2005 (with rating curve errors**
 628 **accounted for).**

629

630

630

631

Catchment (area)	Systematic period		Historical period	
	Q10 +/- IC 90% (m ³ /s)	Q100 +/- IC 90% (m ³ /s)	Q10 +/- IC90% (m ³ /s)	Q100 +/- IC90% (m ³ /s)
Anduze (540 km ²)	1070 +240/-170	2780 +1680/-800	1460 +360/-290	5130 +2650/-1540
Alès (320 km ²)	690 +370/-80	1330 +550/-530	770 +130/-120	1650 +480/-340
Mialet (219 km ²)	250 +90/-60	1170 +1110/-460	270 +80/-60	1250 +770/-420
Saint-Jean (154 km ²)	300 +80/-60	920 +680/-300	360 +100/-70	1480 +900/-480

632

633 **Table 1: 10-year and 100-year quantiles in m³/s estimated on the basis of the systematic and historical**
 634 **periods, and their 90% confidence intervals**

635]

636

637

638

639

640

641

Catchments (area)	Q100 with historical data	Q _{rare} Q _{exc.} (Bressand and Golossov, 1996)	Q _{max} (Stanescu, 2004)	Shyreg (Arnaud and Lavabre, 2007)
Anduze (540 km ²)	9.5	6.2 10.4	7.8	3.8
Alès (320 km ²)	5.2	7.1 11.8	10	5.1
Mialet (219 km ²)	5.7	7.8 13.0	12.8	5.4
Saint- Jean (154 km ²)	9.6	8.5 14.2	13.9	6.4

642

643 **Table 2: Comparison of specific discharge estimates (m³/s.km²) for 100-year quantiles or major floods on**
 644 **the Gardon rivers**

645

646

647

648

648 **Bibliographical references**

649

650 Arnaud P., Lavabre J., Sol B., Desouches C., 2007. Régionalisation d'un générateur de pluies
651 horaires sur la France métropolitaine pour la connaissance de l'aléa pluviographique.
652 *Hydrological Sciences Journal*, 53 (1), 34-47.

653

654 Ayrat P.A., 2005. Contribution à la spatialisation du modèle opérationnel de prévision des
655 crues éclair ALTHAIR, approches spatiale et expérimentale ; application au bassin versant
656 du Gardon d'Anduze. MSc Thesis, University d'Aix Marseille, 311 p.

657

658 Barnes H.H., 1967. Roughness Characteristics of Natural Channels. U.S. Geological Survey,
659 Water Supply Paper 1849.
660 <http://wwwrcamnl.wr.usgs.gov/sws/fieldmethods/Indirects/nvalues/index.htm>

661

662 Brazdil R., Kundzewicz Z.W., Benito G., 2006. Historical hydrology for studying flood risk
663 in Europe. *Hydrological Sciences Journal*, 51 (5), 739-764.

664

665 Bressand F., Golosof G., 1996. Méthode de calcul des débits rares et exceptionnels d'eaux
666 pluviales sur les petits bassins versants naturels situés dans l'arc méditerranéen. DDE
667 (Infrastructure Department) for the Gard region (France), Water and Environment unit, 42 pp.

668

669 Chow, V.T., 1960. Open Channel hydraulics, Mc Graw Hill Book Company, New-York,
670 380p.

671

- 672 Cœur D., Lang M., Paquier A., 2002. L'historien, l'hydraulicien et l'hydrologue et la
673 connaissance des inondations. *La Houille Blanche*, 4/5, 61-66.
674
- 675 Coles, S. G., and E. A. Powell, 1996. Bayesian methods in extreme value modelling: A
676 review and new developments, *Int. Stat. Rev.*, 64, 119-136.
677
- 678 DDE (*Direction Départementale de l'Équipement* – Infrastructure Department) of the Gard
679 region (France), 2003. Validation des relevés hydrométriques de la crue du 08 et 09
680 septembre 2002. SOGREAH internal report, no. 102793, November 2003, 98 pp.
681
- 682 Delrieu G., Kirstetter P-E., Nicol J., Neppel L., 2004. L'événement pluvieux des 08 et 09
683 septembre 2002 dans le Gard : estimation des précipitations par radars et pluviomètres. *La*
684 *Houille Blanche*, 6, 93-98.
685
- 686 Embrecht C., Kluppelberg C., Mikosch T., 1997. *Modelling Extremal Events for Insurance*
687 *and Finance*. Springer-Verlag, Berlin.
688
- 689 Gaume E., Livet M., Desbordes M., Villeneuve J.P., 2004. Hydrological analysis of the river
690 Aude, France, flash flood on 12 and 13 November 1999. *Journal of Hydrology*, 286, 135-154.
691
- 692 Gelman, A., et al., 1995. *Bayesian data analysis*, 526 pp., Chapman & Hall.
693
- 694 Gob F., Jacob N., Bravard J.P., Petit F., 2008. The value of lichenometry and historical
695 archives in assessing the incision of submediterranean rivers from the Little Ice Age in the
696 Ardèche and upper Loire (France). *Geomorphology*, 94, 170-183.

697

698 Hirsh R.M., Stedinger J.R., 1987. Plotting positions for historical floods and their precision.
699 *Water Resources Research*, 22(4), 715-727.

700

701 Huet P., Martin X., Prime J.L., Foin P., Laurain C., Cannard P., 2003. Retour d'expérience
702 des crues de septembre 2002 dans les départements du Gard, de l'Hérault, du Vaucluse, des
703 Bouches du Rhône, de l'Ardèche et de la Drôme. Report of the General Inspectorate for the
704 Environment, Ministry of Ecology, Energy, Sustainable Development and Regional Planning
705 (MEEDDAT), 133 pp.

706 <http://www.ecologie.gouv.fr/-Rapports-de-l-Inspection-generale-.html>.

707

708 ISL Bureau d'Ingenieurs Conseils, 2005. Référentiel hydrologique sur le bassin versant des
709 Gardons. DDE (Infrastructure Department) of the Gard region, internal report.

710

711 Jacquet J., 1959. Les crues d'automne 1958 sur le Vidourle. *Mémoire et travaux de la société*
712 *hydrotechnique de France*, (1)11: 66-82.

713

714 Kuczera, G., 1992. Uncorrelated measurement error in flood frequency inference, *Water*
715 *Resources Research*, 28, 183-188.

716

717 Kuczera, G., 1996. Correlated rating curve error in flood frequency inference, *Water*
718 *Resources Research*, 32, 2119-2127.

719

720 Lang M., Perret C., Renouf E., Sauquet E., Paquier A., 2006. Incertitudes sur les débits de
721 crue. *La Houille Blanche*, 6, 33-41

722

723 Llasat C., Barriendos M., Barrera A., Rigo T., 2005. Floods in Catalonia (NE Spain) since the
724 14th century. Climatological and meteorological aspects from historical documentary sources
725 and old instrumental records. *Journal of Hydrology*, 313, 32-47.

726

727 Martins, E. S., and J. R. Stedinger, 2000. Generalized maximum-likelihood generalized
728 extreme-value quantile estimators for hydrologic data, *Water Resources Research*, 36, 737-
729 744.

730

731 Naulet R., 2002. Utilisation de l'information des crues historiques pour une meilleure
732 prédétermination du risque d'inondation. Application au bassin de l'Ardèche à Vallon Pont
733 d'Arc et à St Martin d'Ardèche. PhD diss., Université Joseph Fourier Grenoble, Université du
734 Québec INRS, Cemagref Lyon, 322 pp.

735

736 Naulet R., Lang M., Ouarda Taha B.M.J., Coeur D., 2005. Flood frequency analysis on the
737 Ardèche river using French documentary sources from the last two centuries. *Journal of*
738 *Hydrology*, 313, 58-78.

739

740 Neppel L., Bouvier C., Vinet F., Desbordes M., 2003. Sur l'origine de l'augmentation des
741 inondations en région méditerranéenne. *Revue des Sciences de l'Eau*, 16 (4), 475-494.

742

743 Neppel L. *et al.*, 2007. InondHis-LR : analyse des précipitations et crues anciennes en région
744 Languedoc-Roussillon. RDT programme, Ministry of Ecology, Energy, Sustainable
745 Development and Regional Planning (MEEDDAT), contract CV04000067, 209 pp.

746

- 747 Marchandise A., 2007. Modélisation hydrologique distribuée sur le Gardon d'Anduze ; étude
748 comparative de différents modèles pluie-débit, extrapolation de la normale à l'extrême et tests
749 d'hypothèses sur les processus hydrologiques, MSc Thesis. University Montpellier II,
750 Montpellier, France.
- 751
- 752 O'Connel, D. R. H., 2005. Nonparametric Bayesian flood frequency estimation, *J. Hydrol.*,
753 313, 79-96.
- 754
- 755 O'Connel, D. R. H., Ostenaar D.A., Levish R., Klinger R.E., 2002. Bayesian flood frequency
756 analysis with paleohydrologic bound data, *Water Resources Research*, 38.
- 757
- 758 Paquier A., Khodashenas S.R., 2002. River bed deformation calculated from boundary shear
759 stress. *Journal of Hydraulic Research*, 40 (5), 603-609.
- 760
- 761 Parent, E., and J. Bernier, 2003. Bayesian POT modeling for historical data, *J. Hydrol.*, 274,
762 95-108.
- 763
- 764 Payrastre O., Gaume E., Andrieu H., 2005. Use of historical data to assess the occurrence of
765 floods in small watersheds in the French Mediterranean Area. *Advances in Geosciences*, 2,
766 313-320.
- 767
- 768 Payrastre O., Gaume E., Andrieu H., 2006. Apport du recueil de données historiques pour
769 l'étude des crues extrêmes de petits cours d'eau ; Etude du cas de quatre bassins versants
770 affluents de l'Aude. *La Houille Blanche*, 6, 79-86.
- 771

- 772 Reis, D. S., and J. R. Stedinger, 2005. Bayesian MCMC flood frequency analysis with
773 historical information, *J. Hydrol.*, 313, 97-116.
774
- 775 Reitan, T., and A. Petersen-Overleir, 2009. Bayesian methods for estimating multi-segment
776 discharge rating curves, *Stochastic Environmental Research and Risk Assessment*. 23(5), 627-
777 642
778
- 779 Renard B., 2006. Détection et prise en compte d'éventuels impacts du changement climatique
780 sur les extrêmes hydrologiques en France. PhD diss., INP Grenoble, Cemagref Lyon, 361 pp.
781
- 782 Renard, B., M. Lang, and P. Bois, 2006a. Statistical analysis of extreme events in a non-
783 stationary context via a Bayesian framework., *Stoch. Environ. Res. Risk Assess.*, 21, 97-112.
784
- 785 Renard B., Garreta V., Lang M., 2006b. An application of Bayesian analysis and MCMC
786 methods to the estimation of a regional trend in annual maxima. *Water Resources Research*,
787 42.
788
- 789 Renouf E., Lang M., Sauquet E., Paquier A., 2005. Contrôle de la qualité des courbes de
790 tarage de la banque HYDRO pour les débits de crue. Cemagref report for the Ministry of
791 Ecology and Sustainable Development (MEDD), 53 pp. + annexes (112 pp.).
792
- 793 Ribatet, M., E. Sauquet, J. M. Gresillon, and T. B. M. J. Ouarda, 2006. A regional Bayesian
794 POT model for flood frequency analysis, *Stoch. Environ. Res. Risk Assess.*, 21, 327-339.
795

796 Sheffer N.A., Rico M., Enzel Y., Benito G., Grodrek T., 2008. The paleoflood record of the
797 Gardon River, France: A comparison with the extreme 2002 flood event. *Geomorphology* 98,
798 71-83, doi:10.1016/j.geomorph.2007.02.034.

799

800 Stanescu V.A., 2004. Le potentiel des grandes crues de l'Europe, leur régionalisation et
801 comparaison. *La Houille Blanche*, 6, 21-25.

802

803 Thyer, M., B. Renard, D. Kavetski, G. Kuczera, S.W. Franks and S.W. Srikanthan, ?? 2009.
804 Critical evaluation of parameter consistency and predictive uncertainty in hydrological
805 modelling: a case study using bayesian total error analysis, *Water Resources Research*, 45.

806 W00B14

807